Dynamics and Attitude Error Analysis for Dock Test System of Small Satellite

Zhang Yuan(张元)*, *Sun Lili*(孙丽丽), *Lai Yinan*(赖一楠), *Dai Ye*(戴野)

School of Mechanical and Power Engineering, Harbin University of Science and Technology, Harbin 150080, P. R. China

(Received 27 February 2014; revised 19 April 2014; accepted 24 April 2014)

Abstract: To analyze the attitude errors of vertical docking test system of small satellite, the static error and kinematic error of test system are considered. The working principle of test system and coordinate of actuator are introduced. The model of friction torque on the joints and torque on docking mechanism are built. Dynamics equation of actuator is built by the Lagrange equation and the Nielsen equation. Under the condition of 24 different angle groups, the calculation of dynamics equation is built by using MATLAB/SIMULINK platform and the kinematic errors of actuator are obtained. The attitude error models of docking mechanism are built. Results shows that the main angle error sources of yaw, row, pitch are not identical. The attitude error of yaw angle can be decreased by compensating the angle error around x axis. The attitude error of row angle mainly originates in the system error, and it can be eliminated by adjusting non-orthogonal degree.

Key words: attitude error; test system; angle errors; dynamics equation

CLC number: V216.8 **Document code**: A **Article ID**: 1005-1120(2015)04-0372-08

0 Introduction

Small spacecrafts are widely used in military, remote communication, disaster prediction and other fields[1-2]. On-orbit dock missions for small aircraft are mainly for fuel supplies, transferring sample in deep-space exploration, failed satellite service, aided-mechanism expansion, assistant-orbiting for satellite, etc. All these avoid transporting people and large quantities, and fuel transport channel need not have big volume. In terms of reliability, cost and flexibility, small dock mechanism has enough advantages over large dock mechanism in the implementation of small satellite dock missions of small carrying capacity and limited installation space. Researches on small dock mechanism with catching characteristics are carried out by space powers, for instance, European Space Agency (ESA)[3] proposed to study the robotic geostationary orbit restorer. German Aerospace Agency[4] supported researches on experimental servicing satellite. Defense Advanced Research Projects Agency (DARPA) supported a demonstration program for frontend robotics to enable near-term demonstration[5].

At present, the dock mechanisms can be classified into several types: "three-jaw" type, "mechanical arm" type, "cone and pole" type, etc. Among them, "three-jaw" type dock mechanism[6] has the least impact force, the lowest velocity and angular velocity in docking. Based on the developed "three jaw type" dock mechanism, a series of work have been done to perform the dynamics simulation of a test system.

In the capture and dock processes of "three jaw type" mechanism[7], the dynamics contact[8] between locking jaws of the active dock mechanism (ADM) and passive dock mechanism (PDM) generates action and reaction forces, which will affect test system and attitude angle

* **Corresponding author**: Zhang Yuan, Professor, E-mail: zhangyuan1966@163.com.

How to cite this article: Zhang Yuan, Sun Lili, Lai Yinan, et al. Dynamics and attitude error analysis for dock test system of small satellite[J]. Trans. Nanjing U. Aero. Astro., 2015,32(4):372-379.
http://dx.doi.org/10.16356/j.1005-1120.2015.04.372

through dock mechanism. In this paper, the errors of attitude angle for docking mechanism are discussed under the influence of the static error and kinematic error[9].

1 Composition and Principle of Vertical Dock Test System

The whole vertical dock test system is divided into a passive test system and an active test system. As shown in Fig. 1, the passive test system is used to install the PDM, thus realizing the rotation around z axis (yaw), x axis (roll), and y axis (pitch), as well as the vertical motion along y direction. The passive test system is mainly composed of a traction counterweight mechanism, a moving end, a hanger frame, a spherical joint bearing, etc. In the active test system, the ADM realizes horizontal movement along x, z directions. The active test system mainly consists of double-rail mobile mechanism.

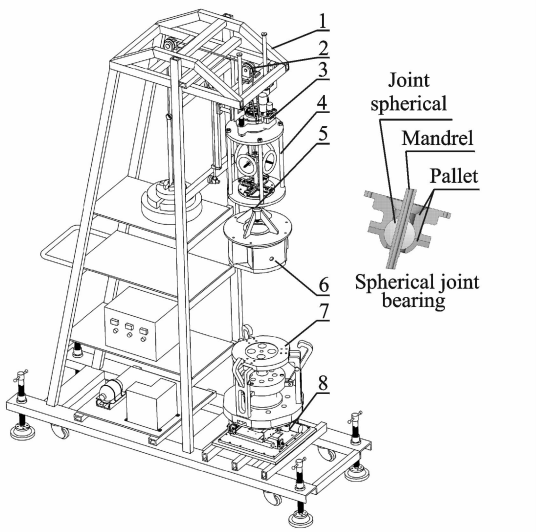

1. Frame; 2. Traction counterweight mechanism; 3. Moving end; 4. Hanger frame; 5. Spherical joint bearing; 6. Passive dock mechanism; 7. Active dock mechanism; 8. Double-rail mobile mechanism

Fig. 1 Vertical dock test system

Experiment processes are stated as follows. Firstly, ADM and PDM are respectively installed on the counter flange of dock test system. Secondly, according to the initial conditions, the location processes are stated as follows. The balance of vertical displacement is realized by adding or reducing counter weight. The balance of the roll and pitch motion are realized by adjusting angle of spherical joint bearing and controlling rotation of motor to initialize yaw angle and horizontal movement along x, z direction. When initialize settings are finished, test system should be in the passive mode state and three locking jaw should be in opening state completely. Finally, the process of contact and capture of dock mechanism are completed and dock driven by motor is realized.

2 Dynamics Model of Contact Impact System

Researches[10-12] on space dock dynamics simulation have been carried out at home and abroad, which provide subsequent researches with important reference value. But most of the present related researches are concentrated on Stewart simulation test system[13-14] and dock mechanism of androgynous and peripheral type with differential cushion damping system. The dock process of test system studied in this paper is realized by recombination processes of several degree of freedom motions, which is realized by different motion modules independently. It is known that the joint spherical in Fig. 1 plays a crucial role in transferring acting force. Dynamics model of actuator is attempted to be built in this paper.

2.1 Introduction to dock process

The dock process of three-jaw dock mechanism is shown in Fig. 2. Before dock, locking jaw 3 is located in envelope zone of PDM. As dock system meets dock initial conditions, threaded rod 5 driven by controlling motor rotates. Thread lifting panel 4 is forced to move down, and three locking jaws simultaneously shift down and close gradually. Meanwhile, the PDM is firmly captured, and attitude deviations are adjusted. Finally, the whole system completes connection locking.

2.2 Coordinate definition of actuator

As illustrated in Fig. 3, the actuator is composed of hanger frame 1, mandrel 2, angle ruler 3, flange 4 and spherical joint 5. This mechanism has three rotational degrees of freedom, the ran-

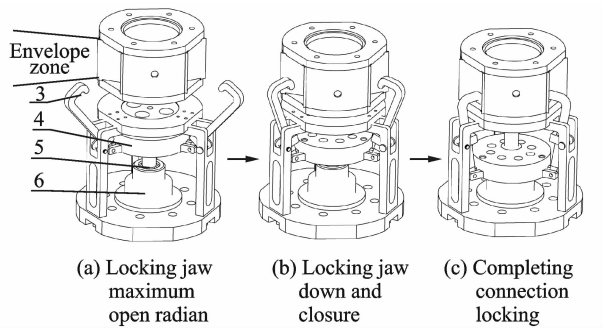

Fig. 2 Dock process

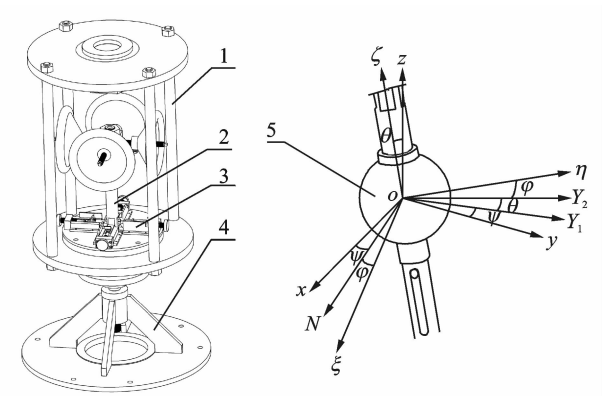

Fig. 3 Coordinate definition of actuator

ges of which are 0—10°.

$Oxyz$ is the static coordinate. The moving coordinate $o\xi\eta\zeta$ is fastened to spherical joint. The origin point of the $Oxyz$ coordinate is located at the centre of spherical joint. The ζ axis is along the axes of mandrel. In the initial state, the moving coordinate $o\xi\eta\zeta$ coincides with $Oxyz$, and the positive direction of ξ, η, ζ are the same with x, y, z.

In order to obtain the space position of mechanism, Euler angles φ, θ, ψ are defined as the generalized displacements. First, the mandrel and the hanger frame rotate along z axis and reach the NY_1z coordinate. Second, the mandrel rotates along the N axis and reaches the $NY_2\zeta$ coordinate. Third, the hanger frame rotates along ζ axis and reaches the $\xi\eta\zeta$ coordinate. The coordinate transformation is described as

$$\begin{bmatrix} x \\ y \\ z \end{bmatrix} = \begin{bmatrix} \cos\psi_1\cos\theta_1 & \sin\theta_1\cos\psi_1\sin\varphi_1 - \sin\psi_1\cos\varphi_1 & \cos\theta_1\sin\psi_1\cos\varphi_1 + \sin\psi_1\sin\varphi_1 \\ \sin\psi_1\cos\theta_1 & \sin\psi_1\sin\varphi_1\sin\theta_1 + \cos\psi_1\cos\varphi_1 & \sin\theta_1\sin\psi_1\sin\varphi_1 - \cos\psi_1\sin\varphi_1 \\ -\sin\theta_1 & \cos\theta_1\sin\varphi_1 & \cos\varphi_1\cos\theta_1 \end{bmatrix} \begin{bmatrix} \xi \\ \eta \\ \zeta \end{bmatrix} \tag{1}$$

which is simplified by

$$\boldsymbol{P} = \boldsymbol{C}\boldsymbol{P}_0$$

2.3 Friction torque of spherical joint

In the process of rotation, the direction of friction torque between spherical joint and pallet is contrary to the rotation direction, as shown in Fig. 4. According to the Hertz elastic deformation theory, the normal stress p of contact surface is in accordance with cosine curve, that is $p = p_0\cos\alpha$, where p_0 is the normal stress of point A and α the angle between ζ axis and radius of arbitrary point on the spherical surface. As $\sum F_\zeta = 0$,

$$Q \cdot \cos\theta = \int_\zeta p_\zeta \cdot \mathrm{d}s = \int_0^{\alpha_1} 2\pi R^2 p_0 \sin\alpha\cos^2\alpha \mathrm{d}\alpha \tag{2}$$

The normal stress distribution rule of contact surface is

$$p_0 = 3Q\cos\theta / 2\pi R^2 (1 - \cos^3\alpha_1) \tag{3}$$

The friction torque is described as

$$M_\xi = \int \mu p = \int_\beta^{\alpha_1} \mu \frac{3Q\cos\theta \cdot \cos\alpha}{2\pi R^2 (1 - \cos^3\alpha_1)} 2\pi R^2 \sin\alpha \cdot \mathrm{d}\alpha \cdot R \tag{4}$$

where r is the mandrel radius. Substitute $\beta = \arcsin r/R$ into Eq. (4).

$$M_\xi = \frac{3\mu QR \cdot \cos\theta \cdot (\cos 2\beta - \cos 2\alpha_1)}{4(1 - \cos^3\alpha_1)} \tag{5}$$

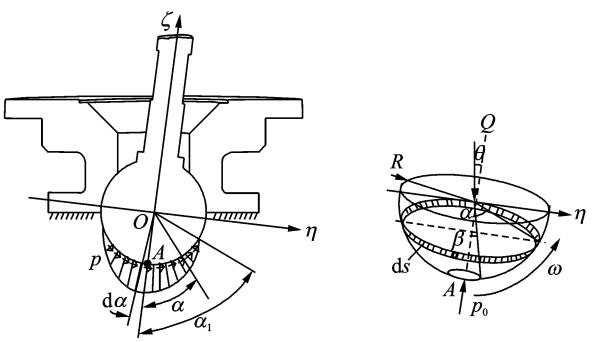

Fig. 4 Friction torque of spherical joint

2.4 Contact force and moment

For the three-jaw dock mechanism, when in the test there exists angular deviation relative to static coordinate system, gradually-closing locking jaws firmly grasp passive dock mechanism and adjust posture deviation under the function of three V-type guide grooves. Finally, the locking

jaws slip into the bottom of V-type guide grooves, and PDM is dragged to ADM simultaneously.

The contact type is divided in two parts: (1) turn angle is yaw angle ψ, named the front impact; (2) turn angle is roll angle φ or pitch angle θ, named the oblique impact.

Fig. 5 shows the force analysis of PDM in $X'OZ'$. $F_n(n=1, 2, 3)$ is the contact force projection over $X'OZ'$, applied by the locking jaw. $F_n(n=1, 2, 3)$ can be decomposed into the force along groove interface and the force perpendicular to groove interface.

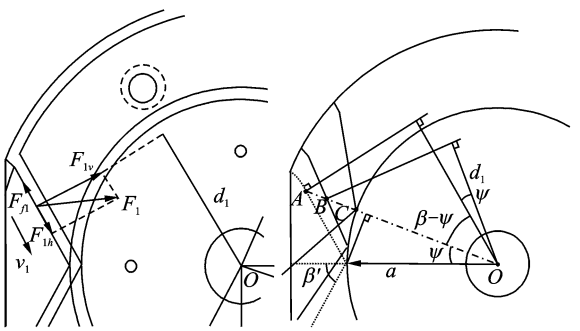

Fig. 5 Force analysis and motion trail of locking jaw

As shown in Fig. 5, $\boldsymbol{r}_{AC}$ is the total displacement of jaw under $X'OY'$ coordinate. Assume that after a few seconds, the jaw reaches point B, and the mandrel rotates $\Delta\psi$ angle. $\boldsymbol{v}_0$ is the radial velocity of jaw. The torque can be described as

$$\begin{cases} M_v = 3F_v \cdot d_1 \\ d_1 = (l_{AO} - v_o t) \cdot \cos(\beta' - \psi + \Delta\psi) \\ l_{AO} = \dfrac{a\sin\psi}{\tan(\beta' - \psi)} + a\cos\psi \\ F_v = F_1 \cdot \sin(\beta' - \psi + \Delta\psi) \end{cases} \tag{6}$$

$F_n(n=1, 2, 3)$ is mainly determined by equivalent stiffness and damping characteristics. F_n and δ satisfy the following equation

$$\delta = \left(\frac{9F_n^2}{16ER^2}\right)^{\frac{1}{3}} \tag{7}$$

where

$$\frac{1}{R} = \frac{1}{R_1} + \frac{1}{R_2} \tag{8}$$

$$\frac{1}{E} = \frac{(1-\mu_1^2)}{E_1} + \frac{(1-\mu_2^2)}{E_2} \tag{9}$$

Here, R_1, R_2 are the curvature radii on impact point of two objects; E_1, E_2 the material elasticity moduli; and μ_1, μ_2 the material Poisson ratio respectively.

Impact process is accompanied by energy losses, which is created by damping characteristics. So this paper adopts a model as

$$F_n = k\delta^n + D\dot{\delta} \tag{10}$$

where k is the equivalent stiffness, $k=1.0\times10^5$. δ, $\dot{\delta}$ are the penetration depth and the relative movement speed, respectively. D is the damping parameter and generally it is (0.1%—1%) k, here $D=100$. n is the stiffness contribution index, for metal, $n=1.3$—1.5, here being 1.5.

2.5 Dynamics model of mandrel and hanger frame

Under the $O\xi\eta\zeta$ coordinate, the mandrel rotates around ξ axis. Under the $Oxyz$ coordinate, the mandrel and hanger frame rotate around z axis. Angular displacement is taken as generalized displacement, that is

$$u_1 = \varphi, \quad u_2 = \theta, \quad u_3 = \psi \tag{11}$$

The torque M_ψ around ψ axis includes $M_{\psi 1}$ and $M_{\psi 2}$, which act on the hanger frame and the mandrel, respectively.

p, q, r are the projections of absolute angular velocity vector $\boldsymbol{\omega}$ of mandrel, which have relationships with generalized velocity.

$$\begin{cases} p = \dot{\psi}\sin\theta\sin\varphi + \dot{\theta}\cos\varphi \\ q = \dot{\psi}\sin\theta\cos\varphi - \dot{\theta}\sin\varphi \\ r = \dot{\psi}\cos\theta + \dot{\varphi} \end{cases} \tag{12}$$

J_z is the rotational inertia of hanger frame around z axis. A, B, C are the rotational inertias of mandrel around ξ, η, ζ axes. The kinetic energy T_1 of hanger frame and T_2 of mandrel can be described as

$$\begin{cases} T_1 = \dfrac{1}{2}J_z\dot{\psi}^2 \\ T_2 = \dfrac{1}{2}Ap^2 + \dfrac{1}{2}Bq^2 + \dfrac{1}{2}Cr^2 \end{cases} \tag{13}$$

The dynamics equation can be obtained by using the Lagrange equation.

$$J_z\ddot{\psi} = M_{\psi 1} \tag{14}$$

T_2 can be described as

$$T_2=\frac{1}{2}A(\dot{\psi}\sin\theta\sin\varphi+\dot{\theta}\cos\varphi)^2+\frac{1}{2}B(\dot{\psi}\sin\theta\cos\varphi-\dot{\theta}\sin\varphi)^2+\frac{1}{2}C(\dot{\psi}\cos\theta+\dot{\varphi})^2 \tag{15}$$

The Nelson equation applied for φ,θ,ψ can be described as

$$\frac{\partial\dot{T}}{\partial\dot{\psi}}-2\frac{\partial T}{\partial\psi}=M_{\psi 1}$$
$$\frac{\partial\dot{T}}{\partial\dot{\theta}}-2\frac{\partial T}{\partial\theta}=M_{\theta}$$
$$\frac{\partial\dot{T}}{\partial\dot{\varphi}}-2\frac{\partial T}{\partial\varphi}=M_{\varphi}$$

Dynamics differential equations of mandrel are obtained from Eq. (15).

$$\begin{cases}(A\sin^2\theta+J_z)\ddot{\psi}=(C-2A\sin\theta)\dot{\psi}\dot{\theta}\cos\theta+C\dot{\varphi}\dot{\theta}\sin\theta+M_{\psi}-M_{\varphi}\cos\theta\\ A\ddot{\theta}=(A-C)\dot{\psi}^2\sin\theta\cos\theta-C\dot{\psi}\dot{\varphi}\sin\theta+M_{\theta}\\ AC\ddot{\varphi}\sin^2\theta=\dot{\psi}\dot{\theta}(AC\sin\theta+AC\sin\theta\cos^2\theta-C^2\cos^2\theta)-C^2\dot{\varphi}\dot{\theta}\sin\theta\cos\theta+(A\sin^2\theta+C\cos^2\theta)M_{\varphi}-CM_{\psi}\cos\theta\end{cases} \tag{16}$$

Define

$$\ddot{\boldsymbol{Y}}=(\ddot{\varphi},\ddot{\theta},\ddot{\psi})^{\mathrm{T}}$$
$$\boldsymbol{M}=(M_{\varphi},M_{\theta},M_{\psi})^{\mathrm{T}}$$

where

$$M_{\theta}=M_x-M_{\zeta}$$
$$M_{\theta}=M_y-M_{\zeta}$$

Here, M_x, M_y are the torques of PDM applied by the locking jaw. Eq. (16) can be described as

$$\boldsymbol{f}(X_1)\ddot{\boldsymbol{Y}}=\boldsymbol{g}(X_1,X_2)+\boldsymbol{h}(X_1)\cdot\boldsymbol{M} \tag{17}$$

where

$$\boldsymbol{f}(X_1)=\begin{bmatrix}AC\sin^2\theta+J_z & 0 & 0\\ 0 & A & 0\\ 0 & 0 & A\sin^2\theta\end{bmatrix}$$

$$\boldsymbol{h}(X_1)=\begin{bmatrix}A\sin^2\theta+C\cos^2\theta & 0 & -C\cos\theta\\ 0 & 1 & 0\\ -\cos\theta & 0 & 1\end{bmatrix}$$

$$\boldsymbol{g}(X_1,X_2)=\begin{bmatrix}\dot{\psi}\dot{\theta}(AC\sin\theta+AC\sin\theta\cos^2\theta-C^2\cos^2\theta)-C^2\dot{\varphi}\dot{\theta}\sin\theta\cos\theta\\ (A-C)\dot{\psi}^2\sin\theta\cos\theta-C\dot{\psi}\dot{\varphi}\sin\theta\\ (C-2A\sin\theta)\dot{\psi}\dot{\theta}\cos\theta+C\dot{\varphi}\dot{\theta}\sin\theta\end{bmatrix}$$

3 Simulation Flow

In Eq. (5), $\mu=0.4$, $Q=60$ N, $R=0.04$ m, mandrel radius $r=0.014$ m, $\alpha_1=\pi/2$. The radial velocity of locking jaw $v_0=0.001$ m/s. The angle of V-type guide groove is 120°. In Eq. (6), $a=260$ mm.

In Eq. (13), $J_z=3.95$ kg·m^2, rotational inertias of mandrel is

$$\boldsymbol{J}=\begin{bmatrix}37.78 & 0 & 0\\ 0 & 3.75 & 0\\ 0 & 0 & 37.78\end{bmatrix}$$

The simulation model is built by using the MATLAB/SIMULINK platform. In order to obtain the motion errors of different angle, the angles of 24 groups are selected, as shown in Table 1.

Table 1 Angles of 24 groups (°)

Angle	Group			
ψ_1	2°	4°	6°	10°
θ_1	0	0	0	0
	2	2	2	2
	4	4	4	4
	6	6	6	6
	8	8	8	8
	10	10	10	10

Table 2 shows the simulation results of different angles.

Table 2 Simulation results (°)

θ_1		ψ_1			
		2°	4°	6°	10°
0°	ψ	2.000 1	4.002 1	6.001 6	10.001 1
	θ	0.000 1	0.002 0	0.003 2	0.005 3
2°	ψ	2.000 1	4.001 9	6.003 2	10.002 5
	θ	2.002 5	2.005 1	2.003 9	2.006 7
4°	ψ	2.003 1	4.003 9	6.006 8	10.003 6
	θ	4.006 5	4.003 2	4.003 8	4.005 4
6°	ψ	2.003 8	4.004 1	6.005 7	10.004 3
	θ	6.009 1	6.003 5	6.004 4	6.003 9
8°	ψ	2.004 0	4.004 9	6.006 0	10.006 2
	θ	8.008 3	8.000 1	8.002 6	8.004 1
10°	ψ	2.006 3	4.006 7	6.005 8	10.005 2
	θ	10.006 5	10.001 4	10.003 1	10.022 5

4 Error Analysis of Attitude Angle

Fig. 6(a) shows the coordinate of gravity center of docking mechanism. Static coordinate $Ox'y'z'$ rotates γ(yaw), α(row), β(pitch) degrees around z', x_1', y_1 axes, respectively to coordinate $Ox_1y_1z_1$, where the three angles are the corresponding attitude angles. The coordinate

transformation is described as

$$\begin{bmatrix} x' \\ y' \\ z' \end{bmatrix} = \begin{bmatrix} \cos\gamma\cos\alpha & -\cos\gamma\sin\alpha\sin\beta+\sin\gamma\cos\beta & \cos\gamma\sin\alpha\sin\beta+\sin\gamma\cos\beta \\ \sin\alpha & \cos\alpha\cos\gamma & -\cos\alpha\sin\beta \\ -\sin\gamma\cos\alpha & \cos\gamma\sin\beta+\sin\gamma\sin\alpha\cos\beta & -\sin\gamma\sin\alpha\sin\beta+\cos\gamma\cos\beta \end{bmatrix} \begin{bmatrix} x_1 \\ y_1 \\ z_1 \end{bmatrix} \tag{18}$$

namely,

$$\boldsymbol{P}' = \boldsymbol{A}\boldsymbol{P}_1$$

The elements in Eq. (1) are equal to elements in Eq. (18).

$$\begin{cases} \gamma = \arctan(\tan\psi_1 \cdot \dfrac{1}{\cos\theta_1}) \\ \alpha = \arcsin(\sin\theta_1 \cdot \cos\psi_1) \\ \beta = \arctan(\dfrac{\tan\varphi_1 - \tan\theta_1\sin\psi_1}{1+\tan\varphi_1\tan\theta_1\sin\psi_1}) \end{cases} \tag{19}$$

If $\tan\tilde{\beta} = -\tan\theta_1\sin\psi_1$, $\tilde{\beta}$ is the associated tilt angle of θ_1 and ψ_1.

$$\beta = \varphi_1 + \tilde{\beta}$$

If actuator generates angular error, the attitude angles are

$$\begin{cases} \gamma = \arctan[\tan(\psi_1+\Delta\psi_1) \cdot \dfrac{1}{\cos(\theta_1+\Delta\theta_1)}] \\ \alpha = \arcsin[\sin(\theta_1+\Delta\theta_1)\cos(\psi_1+\Delta\psi_1)] \\ \beta = \varphi_1 - \arctan[\tan(\theta_1+\Delta\theta_1)\sin(\psi_1+\Delta\psi_1)] \end{cases} \tag{20}$$

Let $\varphi_1 = 0$ since φ_1 does not influence the attitude angle error ranges.

Eq. (20) is the formula to calculate actual attitude angles of docking mechanism under the influence of angular error. In addition, the non-orthogonal degree exists in the coordinate $Oxyz$ caused by normal wear, installation errors, manufacture errors, and so on. As shown in Fig. 6(b), the angles between z axis and x, y, z' axes are $\pi/2+\delta_1$, δ_3, and $\pi/2+\delta_2$, respectively.

$$\cos^2(\frac{\pi}{2}+\delta_1) + \cos^2\delta_3 + \cos^2(\frac{\pi}{2}+\delta_2) = 1$$

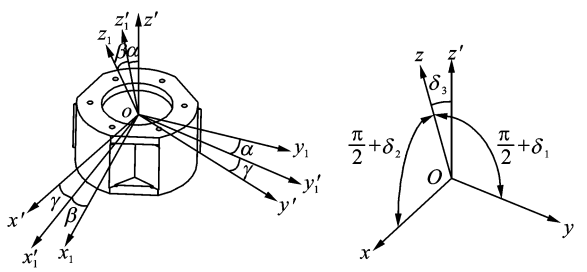

(a) Rotation sequence of $Ox'y'z'$ (b) Non-orthogonal degree of actuator

Fig. 6 Coordinates

Eq. (21) can be obtained from the first rotation in Fig. 3.

$$\begin{bmatrix} x \\ y \\ z \end{bmatrix} = \begin{bmatrix} \cos\psi_1 & -\delta_1(1-\cos\psi_1)+\delta_2\sin\psi_1 & \sin\psi_1 \\ -\delta_1(1-\cos\psi_1)+\delta_2\sin\psi_1 & 1 & -\delta_2(1-\cos\psi_1)+\delta_1\sin\psi_1 \\ \sin\psi_1 & -\delta_2(1-\cos\psi_1)+\delta_1\sin\psi_1 & \cos\psi_1 \end{bmatrix} \begin{bmatrix} n \\ y_1 \\ z \end{bmatrix} \tag{21}$$

Eq. (22) can be obtained from the simultaneous equations of Eq. (21) with the other two rotation transformational matrixes.

$$\begin{bmatrix} x \\ y \\ z \end{bmatrix} = \boldsymbol{E} \begin{bmatrix} \xi \\ \eta \\ \zeta \end{bmatrix} \tag{22}$$

$\boldsymbol{E}$ is the matrix multiplication of the three rotations, whose elements are equal to elements of Eq. (18).

$$\begin{cases} \tan\gamma = \dfrac{\tan\psi_1}{\cos\theta_1} \cdot \dfrac{1}{1+e_1} \\ \sin\alpha = \sin\theta_1 \cdot \cos\psi_1 - e_2 \\ \tan\beta = \tan(\varphi_1+\tilde{\beta}) \\ \tan\tilde{\beta} = -\dfrac{\sin\psi_1\tan\theta_1 + e_3}{1-e_4} \end{cases} \tag{23}$$

where

$$\begin{cases} e_1 = \tan\theta_1[\delta_1(1-\cos\psi_1)/\cos\psi_1 + \delta_2\tan\psi_1] \\ e_2 = \cos\theta_1[\delta_1(1-\cos\psi_1)+\delta_2\sin\psi_1] \\ e_3 = \delta_1\sin\psi_1 - \delta_2(1-\cos\psi_1) \\ e_4 = \tan\theta_1[\delta_1(1-\cos\psi_1) - \delta_2\sin\psi_1] \end{cases} \tag{24}$$

From Eqs. (23), (24), for the given θ_1 and ψ_1, e_1 and e_2 attain the maximum values when δ_1 and δ_2 have the same sign and reach the maximum value (d) of non-orthogonal degree. Thus the attitude angle errors of γ and α are maximized. While e_3 and e_4 reach the maximum values when δ_1 and δ_2 have the opposite sign, the absolute values are the maximums of non-orthogonal degree. Therefore, the attitude angle error of β goes for a maximum value.

$$e_1' = \left(\tan\theta_1 - \tan\theta_1\tan\psi_1 - \frac{\tan\theta_1}{\cos\psi_1}\right) d$$

$$e_2' = (\cos\theta_1\cos\psi_1 - \sin\psi_1\cos\theta_1 - 1)\, d$$

$$e_3' = (1 - \cos\psi_1 + \sin\psi_1) d$$

$$e_4' = d\tan\theta_1(1 - \cos\psi_1 + \sin\psi_1)$$

The attitude angles can be described as

$$\begin{cases}\gamma = \arctan\left(\dfrac{\tan\psi_1}{\cos\theta_1} \cdot \dfrac{1}{1+e_1'}\right) \\ \alpha = \arcsin(\sin\theta_1 \cdot \cos\psi_1 - e_2') \\ \beta = \varphi_1 + \arctan\left(-\dfrac{\tan\theta_1 \sin\psi_1 + e_3'}{1-e_4'}\right)\end{cases} \tag{25}$$

The maximal attitude angle deviating from a nominal value can be obtained by Eq. (20) and Eq. (25). The attitude angles can be obtained by taking angle errors into Eq. (26), here $d = 30''$. Table 3 shows the attitude errors of γ and α. Fig. 7 is the plot of the maximal errors of γ, α and β.

$$\begin{cases}\gamma = \arctan\left[\dfrac{1}{1+e_1'}\tan(\psi_1 + \Delta\psi) \cdot \dfrac{1}{\cos(\theta_1 + \Delta\theta)}\right] \\ \alpha = \arcsin[\sin(\theta_1 + \Delta\theta)\cos(\psi_1 - \Delta\psi) - e_2'] \\ \beta = (\varphi_1 - \Delta\varphi) - \arctan\dfrac{\tan(\theta_1 + \Delta\theta)\sin(\psi_1 + \Delta\psi) + e_3'}{1-e_4'}\end{cases} \tag{26}$$

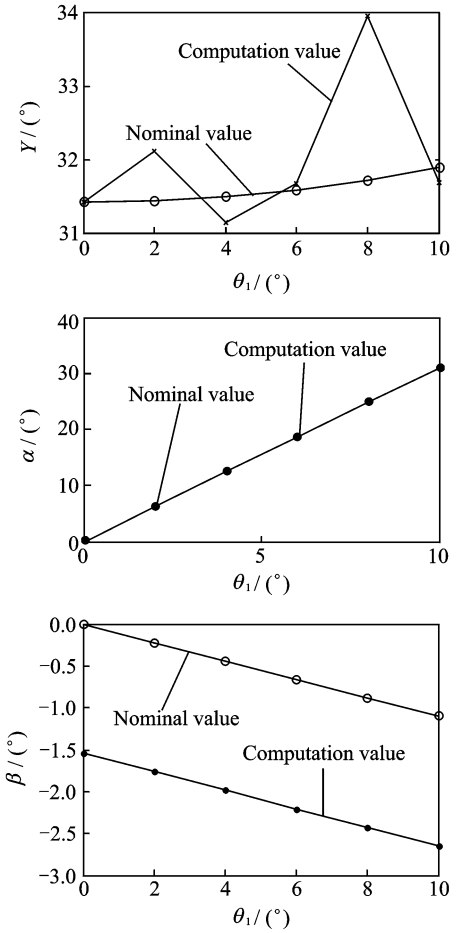

Fig. 7 Actual attitude angle

In Table 3, the deviation variation trends of different ψ_1 values are the same. In Fig. 7, with the same non-orthogonal degree, the angle errors influence γ significantly. The graph of γ is similar to a sine curve. When ψ_1 is given, the deviation of γ reaches its maximum at $\psi_1 = 2°$, $\theta_1 = 8°$. The attitude angle errors of γ can be decreased by compensating the error of angle θ_1. The actual value and nominal value of α are virtually equal, which indicates that the attitude error of α mainly originates in system error. In this case, if δ_1 and δ_2 can be measured, and the exact value of attitude angle can be obtained, then the system error can be eliminated. The attitude errors of β are inversely proportional to ψ_1. When $\psi_1 = 2°$, its maximum value $\Delta\beta = 1.544\ 9°$ is obtained.

Table 3 Attitude errors (°)

θ_1		ψ_1 2°	4°	6°	10°
0°	$\Delta\gamma$	0.003 1	0.003 0	0.003 4	0.003 8
	$\Delta\alpha$	0.056 4	0.111 4	0.168 1	0.286 3
2°	$\Delta\gamma$	0.284 3	0.362 9	−0.352 2	0.682 7
	$\Delta\alpha$	0.057 3	0.112 3	0.169 1	0.287 3
4°	$\Delta\gamma$	−0.150 6	−0.178 4	0.179 2	−0.354
	$\Delta\alpha$	0.060 1	0.115 1	0.171 8	0.290 1
6°	$\Delta\gamma$	0.022 4	0.051 8	−0.063 6	0.083 3
	$\Delta\alpha$	0.064 7	0.119 7	0.176 4	0.294 6
8°	$\Delta\gamma$	0.971 2	1.206 2	−1.075 8	2.233 6
	$\Delta\alpha$	0.071 1	0.126 2	0.182 9	0.301 1
10°	$\Delta\gamma$	−0.107 5	−0.098 2	0.074 3	−0.212 5
	$\Delta\alpha$	0.079 6	0.134 6	0.191 3	0.309 5

5 Conclusions

According to the work principle of actuator, static coordinate and moving coordinate are introduced. Based on the Herz elastic deformation theory, the model of friction torque on the joints and torque on the docking mechanism are built. Dynamics equation of actuator is obtained by the Lagrange equation and the Nielsen equation.

Dynamics simulation model is developed by using the MATLAB/SIMULINK platform. The attitude error model of docking mechanism is built under the influence of static error and kinematic error. Kinematic errors of actuator are obtained. From the calculation results, main error sources of yaw, row, pitch are not identical. Fi-

nally, the methods to reduce the attitude errors are put forward.

Acknowledgements

This work was supported by National Natural Science Foundation of China (No. 51375125), the Foundation for Distinguished Young Scholars of Heilongjiang Province, China (No. JC201111), and the Program for New Century Excellent Talents in University (No. NCET10-0146).

References:

[1] Ennico K, Shirley M, Colaprete A, et al. The lunar crater observation and sensing satellite (LCROSS) payload development and performance in flight[J]. Space Science Reviews, 2012,167(1/2/3/4):1-47.

[2] Bhatia A, Goehner K, Sand J, et al. Sensor and computing resource management for a small satellite [C]// Aerospace Conference, 2013 IEEE. [S. l.]: IEEE, 2013:1-8.

[3] ESA. Robotic geostationary orbit restorer[EB/OL]. http:// www. esa. int/TEC/Robotics/SEMTWLKKKSE. html. [2010-04-03].

[4] Hirzinger G, Landzettel K, Brunner B, et al. DLR's robotics technologies for on orbit servicing[J]. Advanced Robotics, 2004,18:139-174.

[5] DARPA Tactical Technology Office. Front-end robotic enabling near term demonstrations project page [EB/OL]. http:// www. darpa. mil/tto/programs/frend. htm. [2010-04-03].

[6] Zhang Y, Wang J, Song Y, et al. Dynamic simulation analysis for docking mechanism of on-orbit-servicing satellite[J]. Applied Mechanics and Materials, 2014,487:313-318.

[7] Zhao M J. Key technical study of ground six degrees of freedom platform for microsatellite docking mechanism[D]. Harbin, China: Harbin University of Science and Technology, 2011:5-30. (in Chinese)

[8] Xu C L, Wang X W. Efficient numerical method for dynamic analysis of flexible rod hit by rigid ball[J]. Transactions of Nanjing University of Aeronautics & Astronautics, 2012,29(4):338-344.

[9] Zhao H S. Model of flight technical error in symmetrical plane for performance based navigation [J]. Transactions of Nanjing University of Aeronautics & Astronautics, 2011,28(3):246-254.

[10] Li C G, Wang H M, Zhu J Y. Dynamics analysis of 2-DOF spherical parallel mechanism [J]. Transactions of Nanjing University of Aeronautics & Astronautics, 2009,26(2):95-100.

[11] Howsman T G, Glaese J R. Space station docking mechanism dynamic testing[J]. Space Science Reviews, 2008,89(12):168-175.

[12] Shi J W. Study on 6-DOF simulator dynamics for half-physical synthetic docking simulation precision [D]. Shanghai, China: Shanghai Jiaotong University, 2012:29-40. (in Chinese)

[13] Dasgupta B, Mruthyunjaya T S. Closed-form dynamic equations of the general Stewart platform through the Newton-Euler approach[J]. Mechanism and Machine Theory, 1998,33(7):993-1012.

[14] Colebank J E, Jones R D, Pollak R D, et al. SIMSAT: A satellite system simulator and experimental test bed for air force research[R]. Simsat A Satellite System Simulator & Experimental Test Bed for Air Force Research, 1999.

(Executive editor: Zhang Tong)